

Momentum dependence of the N to Δ transition form factors *

C. Alexandrou^a, Ph. de Forcrand^b, H. Neff^c, J. W. Negele^d, W. Schroers^{†d} and A. Tsapalis^{‡a}

^aDepartment of Physics, University of Cyprus, CY-1678 Nicosia, Cyprus

^bETH-Zürich, CH-8093 Zürich and CERN Theory Division, CH-1211 Geneva 23, Switzerland

^cPhysics Department, Boston University, Boston, Massachusetts 02215, USA

^dCenter for Theoretical Physics, Laboratory for Nuclear Science and Department of Physics, Massachusetts Institute of Technology, Cambridge, Massachusetts 02139, USA

We present a new method to determine the momentum dependence of the N to Δ transition form factors and demonstrate its effectiveness in the quenched theory at $\beta = 6.0$ on a $32^3 \times 64$ lattice. We address a number of technical issues such as the optimal combination of matrix elements and the simultaneous overconstrained analysis of all lattice vector momenta contributing to a given momentum transfer squared, Q^2 .

1. Introduction

The N to Δ transition form factors encode important information on hadron deformation and have been studied carefully in recent experiments [1]. In this work we present the first lattice evaluation of the momentum dependence of the magnetic dipole, M1, the electric quadrupole, E2, and the Coulomb quadrupole, C2, transition amplitudes. They are calculated in the quenched approximation on a lattice of size $32^3 \times 64$ at $\beta = 6.0$ with Wilson fermions with sufficient accuracy to exclude a zero value of E2 and C2 at low Q^2 . This accuracy is achieved by applying two novel methods: 1) We use an interpolating field for the Δ that allows a maximum number of statistically distinct lattice measurements contributing to a given Q^2 . 2) We extract the transition form factors by performing an overconstrained analysis of the lattice measurements using all lattice momentum vectors contributing to a given Q^2 value [2].

2. Evaluation of the three-point function

The evaluation of the three-point function $G_\sigma^{\Delta j^\mu N}(t_2, t_1; \mathbf{p}', \mathbf{p}; \Gamma)$ can be done either using the fixed current approach as in previous lattice calculations [3,4] or the fixed sink approach, where the current can couple to the backward

sequential propagator at any time slice t_1 carrying any lattice momentum [5], allowing the evaluation of the form factors at all possible momentum transfers. As shown in Fig. 1, for the same statistics, the errors in M1 in the fixed sink method are almost three times as large as those obtained in the fixed current approach. Therefore in order to make use of the advantages of the fixed sink approach, we must first reduce the errors. We start by modifying the ratio used in ref. [4] so that we do not need to evaluate both $\langle G_\sigma^{\Delta j^\mu N}(t_2, t_1; \mathbf{p}', \mathbf{p}; \Gamma) \rangle$ and $\langle G_\sigma^{N j^\mu \Delta}(t_2, t_1; \mathbf{p}', \mathbf{p}; \Gamma) \rangle$, since this would require two inversions. Instead we use the ratio

$$R_\sigma = \frac{\langle G_\sigma^{\Delta j^\mu N}(t_2, t_1; \mathbf{p}', \mathbf{p}; \Gamma) \rangle}{\langle G_{ii}^{\Delta \Delta}(t_2, \mathbf{p}'; \Gamma_4) \rangle} \left[\frac{\langle G_{ii}^{\Delta \Delta}(t_2, \mathbf{p}'; \Gamma_4) \rangle}{\langle G^{NN}(t_2, \mathbf{p}; \Gamma_4) \rangle} \right]^{1/2} \stackrel{t_2-t_1 \gg 1, t_1 \gg 1}{\Rightarrow} \Pi_\sigma(\mathbf{p}', \mathbf{p}; \Gamma; \mu), \quad (1)$$

in the notation of ref. [4]. We use kinematics where the Δ is produced at rest and so $\mathbf{q} \equiv \mathbf{p}' - \mathbf{p} = -\mathbf{p}$. We fix $t_2/a = 12$ and search for a plateau of $R_\sigma(t_2, t_1; \mathbf{p}', \mathbf{p}; \Gamma; \mu)$ as function of t_1 .

In the fixed sink approach, the index σ of the Δ and projection matrix Γ are fixed and therefore we need to determine the most suitable choice of three-point functions from which to extract the

*Talk presented by C. Alexandrou

†Supported by the Alexander von Humboldt Foundation

‡Supported by the Levendis Foundation

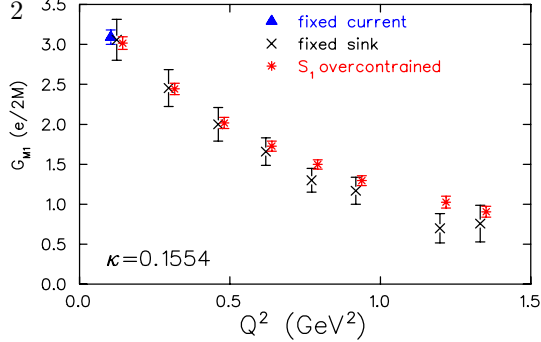


Figure 1. \mathcal{G}_{M1} in Bohr magnetons at $\kappa = 0.1554$. Sachs form factors \mathcal{G}_{M1} , \mathcal{G}_{E2} and \mathcal{G}_{C2} [4]. For example \mathcal{G}_{M1} can be extracted from

$$\Pi_\sigma(\mathbf{q}; \Gamma_4; \mu) = iA\epsilon^{\sigma 4\mu j} p^j \mathcal{G}_{M1}(Q^2) \quad (2)$$

where A is a kinematical coefficient and $\Gamma = \Gamma_4 = \frac{1}{2} \begin{pmatrix} I & 0 \\ 0 & 0 \end{pmatrix}$ in Eq. (1). This leaves 3 choices for σ i.e there are three statistically independent matrix elements yielding \mathcal{G}_{M1} , each requiring a sequential inversion. However, due to the ϵ factor, fixing σ means that only momentum transfers in the other two directions contribute. Instead, if we take the symmetric combination, $S_1(\mathbf{q}; \mu) = \sum_{\sigma=1}^3 \Pi_\sigma(\mathbf{q}; \Gamma_4; \mu)$, momentum vectors in all directions contribute. This combination, which we refer to as sink S_1 , is built into the Δ interpolating field and requires only one inversion. To take full advantage of the number of lattice vectors contributing to a given Q^2 we perform an overconstrained fit by solving the overcomplete set of equations $P(\mathbf{q}; \mu) = D(\mathbf{q}; \mu) \cdot F(Q^2)$ where $P(\mathbf{q}; \mu)$ are the lattice measurements of the ratio of Eq. (1), $F = \begin{pmatrix} \mathcal{G}_{M1} \\ \mathcal{G}_{E2} \\ \mathcal{G}_{C2} \end{pmatrix}$ and, with N being the number of current directions and momentum vectors contributing to a given Q^2 , D is an $N \times 3$ matrix which depends on kinematical factors. We extract the form factors by minimizing

$\chi^2 = \sum_{k=1}^N \frac{1}{w_k^2} \left(\sum_{j=1}^3 D_{kj} F_j - P_k \right)^2$, where w_k are the errors in the lattice measurements, using singular value decomposition of D . In Fig. 1, we compare the results for \mathcal{G}_{M1} using an overconstrained analysis with sink type S_1 to our old analysis with fixed $\sigma = 2$ and $\mu = 3$. The errors with our new analysis are reduced at all values of Q^2 and are now equal to the error obtained using the fixed current approach.

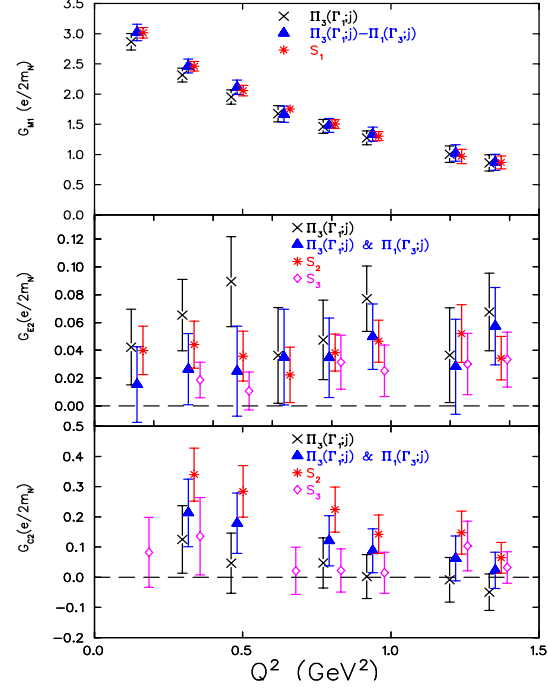


Figure 2. Top: \mathcal{G}_{M1} , middle: \mathcal{G}_{E2} and bottom: \mathcal{G}_{C2} in Bohr magnetons at $\kappa = 0.1554$ using $\Pi_3(\mathbf{q}; \Gamma_1; j)$ (crosses), $\Pi_3(\mathbf{q}; \Gamma_1; j) - \Pi_1(\mathbf{q}; \Gamma_3; j)$ (filled triangles), S_1 or S_2 (asterisks) and S_3 (open circles) and an overconstrained analysis.

Using $\Gamma_k = \frac{1}{2} \begin{pmatrix} \sigma_k & 0 \\ 0 & 0 \end{pmatrix}$ instead of Γ_4 gives another six statistically independent 3-point functions from which \mathcal{G}_{M1} can be extracted:

$$\Pi_\sigma(\mathbf{q}; \Gamma_k; j) = B \left\{ \frac{1}{2} (p_\sigma \delta_{kj} - p_k \delta_{\sigma j}) \mathcal{G}_{M1}(Q^2) - \left[\frac{3}{2} (p_\sigma \delta_{kj} + p_k \delta_{\sigma j}) - \frac{3p_\sigma p_k p_j}{\mathbf{p}^2} \right] \mathcal{G}_{E2}(Q^2) - \frac{(E_N - m_\Delta)}{2m_\Delta} p_j \left(\delta_{\sigma k} - \frac{3p_\sigma p_k}{\mathbf{p}^2} \right) \mathcal{G}_{C2}(Q^2) \right\} \quad (3)$$

where B and C are kinematical coefficients. To isolate the benefits of using S_1 we compare in Fig. 2 \mathcal{G}_{M1} obtained using S_1 to the ones obtained by fixing $\sigma = 3$ and Γ_1 in Eq. (3) [4]. All results are now obtained with the overconstrained analysis using 50 configurations. As can be seen, S_1 produces results with the smallest errors and it is therefore the optimal sink for \mathcal{G}_{M1} .

For the extraction of the quadrupole moments, we consider the symmetric combination $S_2(\mathbf{q}; \mu) = \sum_{\sigma \neq k=1}^3 \Pi_\sigma(\mathbf{q}; \Gamma_k; \mu)$ from which both

\mathcal{G}_{E2} and \mathcal{G}_{C2} can be extracted when the current is in the spatial direction. When the current is in the time direction, S_2 provides a statistically independent way for evaluating \mathcal{G}_{C2} , at no extra cost. Another combination to extract the quadrupole form factors is $S_3 = \Pi_3(\mathbf{q}; \Gamma_3; \mu) - \frac{1}{2}(\Pi_1(\mathbf{q}; \Gamma_1; \mu) + \Pi_2(\mathbf{q}; \Gamma_2; \mu))$, which, unlike S_2 , contributes at the lowest value of Q^2 . As can be seen in Fig. 2, S_2 produces results with smaller errors as compared to those using $\Pi_3(\Gamma_1; j)$ and $\Pi_1(\Gamma_3; j)$ for both E2 and C2. Increasing the the statistics from 50 to 200 configurations brings agreement between S_2 and S_3 for \mathcal{G}_{C2} as well.

3. Results and Conclusions

We analyse 200 configurations at $\kappa = 0.1554$, 0.1558 and 0.1562 corresponding to $m_\pi/m_\rho = 0.64$, 0.59 and 0.50 respectively. We use the nucleon mass at the chiral limit to set the lattice spacing a , obtaining $a^{-1} = 2.04(2)$ GeV. Using the optimal sink S_1 our results for \mathcal{G}_{M1}^* are shown in Fig. 3 as a function of Q^2 , where

$$\mathcal{G}_{M1}^* \equiv \frac{1}{3} \frac{1}{\sqrt{1 + \frac{Q^2}{(m_N + m_\Delta)^2}}} \mathcal{G}_{M1} . \quad (4)$$

Results in the chiral limit are obtained by performing a linear extrapolation in m_π^2 . On the same figure, we also show the experimental values as extracted from the measured cross sections using the phenomenological model MAID [6]. Although the lattice data in the chiral limit lie higher than the MAID data both data sets are well described by the the phenomenological parametrization $\mathcal{G}_a(Q^2) = \mathcal{G}_a(0)(1 + \alpha \exp(-\gamma Q^2)) G_E^p(Q^2)$ for $a = M1, E2$ and $C2$ and $G_E^p(Q^2) = 1/(1 + Q^2/0.71)^2$ is the proton electric form factor. These fits are shown in Fig. 3 by the solid lines.

In Fig. 3, we show the ratios EMR $\equiv R_{EM} = -\frac{\mathcal{G}_{E2}(q^2)}{\mathcal{G}_{M1}(q^2)}$ and CMR $\equiv R_{SM} = -\frac{|\mathbf{q}|}{2m_\Delta} \frac{\mathcal{G}_{C2}(q^2)}{\mathcal{G}_{M1}(q^2)}$. Results in the chiral limit are obtained by performing a linear extrapolation in m_π^2 . As expected, both EMR and CMR become more negative as we approach the chiral limit. The results for EMR are in agreement with experimental measurements whereas CMR is not as negative as experiment at low Q^2 . We believe that CMR is

particularly sensitive to the absence of sea quarks and thus a good probe of unquenching effects.

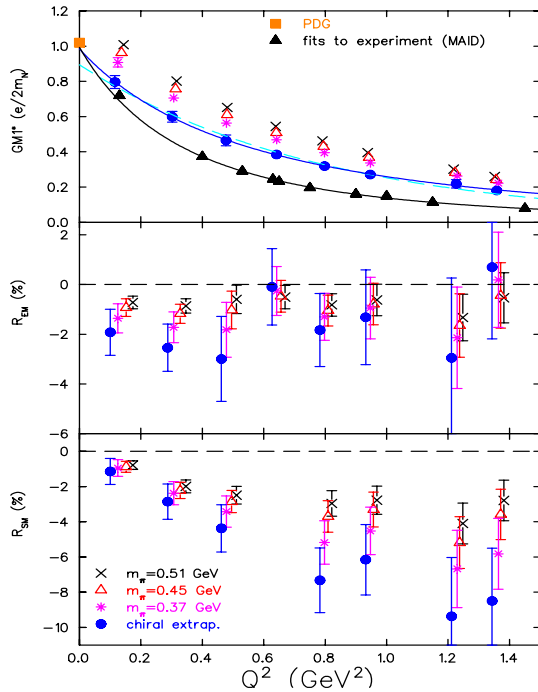


Figure 3. Top: \mathcal{G}_{M1}^* , middle: EMR, bottom: CMR as function of Q^2 at $\kappa = 0.1554$ (crosses), $\kappa = 0.1558$ (open triangles), $\kappa = 0.1562$ (asterisks) and in the chiral limit (filled circles). Filled triangles show \mathcal{G}_{M1}^* extracted from measurements using MAID [6]. The dashed line is a fit to the lattice data using $a \exp(-bQ^2)$.

REFERENCES

1. C.Mertz *et al.*, Phys. Rev. Lett. **86**, 2963 (2001); K. Joo *et al.*, Phys. Rev. Lett. **88** 122001 (2002).
2. LHPC and SESAM collaborations, Ph. Hägler, *et. al.*, Phys. Rev. D**68**, 034505 (2003).
3. D. B. Leinweber, T. Draper, and R. M. Woloshyn, Phys. Rev. D **48**, 2230 (1993).
4. C. Alexandrou, *et. al.*, Phys. Rev. D **69**, 114506 (2004).
5. C. Alexandrou, *et. al.*, Nucl. Phys. (Proc. Suppl.) **129**, 221 (2004); C.Alexandrou, Nucl. Phys. (Proc. Suppl.) **128**, 1 (2004).
6. D. Drechsel, O. Hanstein, S.S. Kamalov and L. Tiator, Nucl. Phys. **A645** 145 (1999).